Applied Catalysis B: Environmental 95 (2010) 78–86

Contents lists available at ScienceDirect

Applied Catalysis B: Environmental

journal homepage: www.elsevier.com/locate/apcatb

Photo-induced carbonation of lime-TiO_2 mortars

Ioannis Karatasios [a], Marios S. Katsiotis [a], Vlassis Likodimos [b], Athanasios I. Kontos [b], Georgios Papavassiliou [a], Polycarpos Falaras [b,*], Vassilis Kilikoglou [a,**]

[a] Institute of Materials Science, National Centre for Scientific Research 'Demokritos', Athens 153 10, Greece
[b] Institute of Physical Chemistry, National Centre for Scientific Research 'Demokritos', 153 10 Aghia Paraskevi Attikis, Athens, Greece

ARTICLE INFO

Article history:
Received 25 September 2009
Received in revised form 30 November 2009
Accepted 9 December 2009
Available online 22 December 2009

Keywords:
Lime
Carbonation
Photocatalysis
TiO_2
Mortars
Conservation
Cultural heritage

ABSTRACT

In this work, titanium dioxide (TiO_2) has been used as an additive in lime binder ($Ca(OH)_2$), in order to benefit from its photocatalytic properties and study both the photocatalytic properties of the produced mixtures and the effect of photocatalytically produced carbon dioxide on the carbonation process of lime. TiO_2 was added in three different portions (3, 6 and 10% w/w) in lime mixtures and their physicochemical and photocatalytic properties were studied and compared to those of a reference, made exclusively of lime. The photocatalytic properties of the mixtures were studied through the photo-oxidation of an organic model pollutant solution (methyl orange) to a colorless form, as well as by studying the microstructure and carbonation depth in different groups of mixtures subjected to photocatalysis cycles in the laboratory and exposed for a 2 month period in the open air (urban environment).

Laboratory results confirmed that lime-TiO_2 composite mixtures exhibit photocatalytic properties in both UV radiation conditions and direct exposure to sunlight. Moreover, analytical results indicated an enhanced carbonation of lime-TiO_2 composites. TiO_2 can be added to lime successfully and can have applications in lime-based mortars used in the conservation of architectural heritage, enhancing their performance against soiling and amenity loss.

1. Introduction

Atmospheric pollution has a major impact on the quality of both the natural and manmade environment, including cultural heritage. As a result, today, many historic buildings and architectural monuments, located in urban or industrial centers are particularly vulnerable to the effect of air pollutants and particulate matter [1,2]. The effect of air pollutants on built heritage is mainly described through the mechanisms of wet and dry deposition processes [3,4] and results in the formation of gypsum ($CaSO_4 \cdot 2H_2O$) compounds on the surface of the monuments [5]. Together with gypsum, particulate matter, aerosols, spores, pollen, organic (OC) and elemental (EC) carbon are usually embedded on the building's surface [6], contributing to the formation of a brownish-gray to black crust [5,7]. In recent decades, the effect of traffic and vehicular emissions has resulted in an increase of the amount of inorganic compounds (such as nitrogen oxides–NOx) emitted in the atmosphere, along with organic ones (volatile organic compounds-VOC's). The latter originate from partially uncombusted fuels, lubricating oils and domestic heating systems and are deposited on the surface of historic monuments and urban buildings [8,9]. The most abundant organic compounds include straight-chain alkanes, ketones, fatty acids, benzene derivatives (alkylbenzenes and alkylmethylbenzenes), terpanes, triterpanes, steranes, polycyclic aromatic hydrocarbons (PAHs) and diterpenoids [1,10,11]. Nowadays, the deposition of the above compounds on building facades results in important aesthetic, economic and ecological implications [11–13].

The development of the black crusts affects more the preservation condition of historic lime-based mortars [14–16], which have been used extensively as protective and decorative material on the external surface of historic buildings. This is attributed to the solubility of their carbonate matrix in acid solutions, the increased solubility of gypsum embedded in crusts and therefore the weakening of the external layers by run-off water, when aqueous methods are used for cleaning. In the case of new, renovation mortars, in addition to the above process their degradation is also affected by the degree of lime carbonation. The carbonation of lime is a very slow, self-limiting process [17–19], and this delay influences its performance, in terms of solubility and

* Corresponding author. Tel.: +30 210 6503644; fax: +30 210 6511766.
** Corresponding author. Tel.: +30 210 6503317; fax: +30 210 6519430.
E-mail addresses: ikarat@ims.demokritos.gr (I. Karatasios), marios.katsiotis@ims.demokritos.gr (M.S. Katsiotis), likodimo@chem.demokritos.gr (V. Likodimos), athkontos@chem.demokritos.gr (A.I. Kontos), gpapav@ims.demokritos.gr (G. Papavassiliou), papi@chem.demokritos.gr (P. Falaras), kilikog@ims.demokritos.gr (V. Kilikoglou).

0926-3373/$ – see front matter © 2009 Elsevier B.V. All rights reserved.
doi:10.1016/j.apcatb.2009.12.011

leaching of the binding material. Compared to calcium hydroxide [$Ca(OH)_2$] ($K_{sp} = 7.9 \times 10^{-6}$ at 25 °C), calcium carbonate ($CaCO_3$) is a compound of lower solubility ($K_{sp} = 2.8 \times 10^{-9}$ at 25 °C) [20]. Thus, in the case of delayed carbonation, the amount of the binding material that is potentially dissolved in aqueous solutions and washed out of the mortar matrix is increased. In order to improve the durability and strength characteristics of lime-based mortars, different approaches have been attempted, aiming to accelerate the carbonation of the binder, including the use of ammonium (bi-)carbonates, carbonic acid esters (carbamates) [21] and poly-amino-phenolic (PAP) oligomers [22]. The use of these compounds can increase considerably the carbonation rate and strength characteristics of lime. However, the rapid evolution of CO_2, that results from ammonium (bi-)carbonates, does not permit the homogeneous carbonation of lime, while the use of carbamates affects the fluidity and workability of the mixtures [21]. Thus, the forced reaction of lime binders with high amounts of CO_2 amounts leads to a modification in the habit, morphology and size of the calcite crystals [23] and therefore, creates differences in the microstructure and porosity of lime mortars.

Aiming to eliminate the effects of air pollutants on the degradation rate of lime-based mortars and, therefore, enhance their durability and service life through an 'environmental friendly' approach, this work investigates the potential of adding titanium dioxide (TiO_2) in lime-mixtures, designed for the conservation of external renders, decorative elements and facades of historic and contemporary buildings.

Driven by its unique photo-induced reactivity together with its environmentally benign properties (non-toxic, non-soluble in water, photostable), and relatively low cost, TiO_2 is regarded as the most efficient and environmentally friendly photocatalyst that has the potential to oxidize virtually all organic pollutants, while at the same time producing no harmful end products when applied at optimum conditions [24]. TiO_2 photocatalysis is characterized by two distinct reaction pathways, the first involving oxidation, from photo-generated holes, and the second involving reduction, from photo-generated electrons, both excited upon UV irradiation with energy exceeding the TiO_2 band gap. The oxidation mechanism, in particular, is primarily based on the formation of hydroxyl radicals through interfacial charge transfer reactions involving the photo-generated holes, occurring at time scales shorter than charge recombination processes at the surface or the bulk of the semiconductor [24]. Hydroxyl radicals are extremely reactive (redox potential as high as 2.7 V at acidic pH), non-selective, and readily attack organic contaminants, which are sequentially transformed to simpler organic molecules that are eventually mineralized to CO_2, H_2O, and inorganic salts. As a consequence, when TiO_2 is used as an additive to a variety of materials, it endows them with photocatalytic and/or self-cleaning properties. Titania has found great use as an additive in construction materials (cement, concrete, tiles and windows) for its sterilizing, deodorizing and anti-fouling properties [25,26]. TiO_2 integrated in construction materials, effectively decomposes or deactivates all types of volatile organic compounds (VOC's) and nitrogen oxides (NOx), while also removing bacteria and other harmful agents. It is apparent that the photocatalysis effect takes place on the surface of the material and, most importantly, that the final decomposition product of most organic compounds is CO_2 and water. In the case of organic pollutants, such as NOx, their oxidation leads to the formation of nitrates [24]. The production of CO_2 indicates that titanium dioxide could be mixed effectively with lime and act beneficially for both photocatalysis and carbonation. The CO_2 produced during the photodecomposition of organic compounds could be dissolved in water, absorbed by the mortar and, thus enhance the carbonation process of the lime binder.

Based on the encouraging results delivered from the addition of TiO_2 in construction materials and especially cement [13,25], this work investigates the effect of titanium dioxide on the physical and mechanical properties of lime binders, the photocatalytic activity or the self-cleaning properties of the mixtures produced, the potential of photo-oxidation in the carbonation process of the above mixtures and, therefore, the ability of new lime-based mortars to maintain their performance requirements and aesthetic characteristics.

2. Experimental

2.1. Materials and test specimens

The effect of TiO_2 on the properties of lime mortars was studied in binary pastes consisted of calcium hydroxide and titania mixed with the appropriate amount of water. Degussa P25 TiO_2 was used as photocatalyst (75% anatase–25% rutile, average primary particle size of 21 nm and BET surface area of 50 ± 15 m^2/g), based on its well established photocatalytic and self-cleaning ability of cement-based construction materials [25,27]. Calcium hydroxide was provided by Fluka - Riedle de Haen (calcium hydroxide ≥96%, calcium carbonate ≤4%), having 2.24 g/cm^3 real density and 14.15 m^2/g surface area.

The properties of lime-TiO_2 pastes were compared to those of a reference mixture consisted only of calcium hydroxide. Titania was added to the initial lime mixture in three different portions (3, 6 and 10% w/w), in order to ensure the presence of a constant amount, evenly distributed within the mass of the mortars and avoid any layering or conglomeration effect (Table 1). For each mixture, the water to binder ratio (w/b) was set to one. The mixtures were moulded in two different types of moulds with dimensions 100 mm × 100 mm × 10 mm and 15 mm × 15 mm × 80 mm and left to dry for 4 weeks at 20 ± 2 °C and 45 ± 5% relative humidity. During drying one of the flat surfaces of the specimens remained in direct contact with the mold, ensuring negligible carbonation. This particular side of the specimens was then used in the experimental processes. After the 4-week period, all the samples were submitted in four different conditions in order to assess the way photocatalysis affects carbonation, as explained in detail below. For the laboratory photocatalytic experiments, thin films were prepared by depositing the lime-TiO_2 pastes on microscopy glass slides using the doctor-blade technique.

Table 1
Mixture proportions of solid compounds (% w/w) and sample codes for binary pastes.

Composition (% w/w)		Treatment			
Lime	TiO_2	Lab conditions/no photocatalysis	M.O. immersion/no photocatalysis	M.O. immersion and photocatalysis	Open air/urban environment
100	0	Ca100_Ref	Ca100_D	Ca100_L	Ca100_Ex
97	3	Ca97T3_Ref	Ca97T3_D	Ca97T3_L	Ca97T3_Ex
94	6	Ca94T6_Ref	Ca94T6_D	Ca94T6_L	Ca94T6_Ex
90	10	Ca90T10_Ref	Ca90T10_D	Ca90T10_L	Ca90T10_Ex

2.2. Microstructure and mechanical properties

The effect of titanium dioxide on the hygric properties and pore characteristics of lime was investigated in specimens cured for 4 weeks. The water absorption coefficient was measured in prismatic specimens of 15 mm × 15 mm × 80 mm, at atmospheric pressure, using a procedure very similar to the one described in EN 1925 [28], in order to fit the actual size of the specimens. Pore characteristics were determined by mercury intrusion porosimetry (MIP), in the range of 2–4.000 nm, using a Quantachrome/Autoscan 60 porosimeter. Moreover, the microstructure of the produced pastes was studied under a FEI/Quanta Inspect D8334 scanning electron microscope, coupled with energy dispersive X-ray analysis (SEM/EDX).

The internal cohesion of the binary cementing material produced was studied through the determination of flexural strength (three point bending test) of prismatic specimens (15 mm × 15 mm × 80 mm) [29]. For the preparation of the prismatic specimens, the binding material was mixed with standard siliceous sand (0–2 mm), with a binder to aggregate ratio of 1/3 (w/w). Three specimens from each mixture were tested in an Instron 1195 testing machine, using a displacement rate of 109 μm/s.

2.3. Photocatalytic activity

The photocatalytic activity of lime-TiO_2 pastes was evaluated by studying the photodegradation of methyl orange (MO) azo-dye, 4-dimethylaminoazobenzene-4'-sulfonic acid sodium salt. Methyl orange was chosen in order to simulate organic pollutants and ensure CO_2 release, as MO can be completely decomposed by TiO_2 under UV irradiation, resulting in the mineralization of this azo-dye and the consequent production of CO_2 [30,31].

Photocatalysis experiments were carried out in round-bottom photocatalytic cells, transparent to wavelengths above 320 nm. The cells were introduced into a laboratory constructed photocatalytic reactor equipped with four F15W/T8 black light tubes (Sylvania GTE) with maximum emission at 350 nm and a power density of about 1.5 mW/cm^2 on the photocatalyst surface [32].

The experiments were performed in the presence of titania-modified lime mixtures, deposited as thin films on microscopy glass slides (surface area of 1.0 cm^2). The composite films (surface area of 1.0 cm^2) were immersed, under continuous stirring, in 4 ml of 2×10^{-5} M MO aqueous solution. Prior to their use, the MO solutions were bubbled with O_2 for 2 h in order to reach dissolved oxygen saturation that promotes the photocatalytic reaction though its electron scavenging function [33,34]. Before UV irradiation, the photocatalyst was immersed into the MO solution and was left in the dark for 2 h to equilibrate the pollutant adsorption on the lime-TiO_2 layers. Analytical determination of the MO concentration during photocatalysis was carried out spectrophotometrically at 466.5 nm (ε_{MO} = 25100 L/mol cm).

2.4. Carbonation monitoring

The effect of CO_2 produced during photo-oxidation on the carbonation of lime-TiO_2 pastes was studied in three groups of specimens, initially cured for four weeks at 20 ± 2 °C and 45 ± 5% relative humidity. The first group (L) was submitted to continuous photo-oxidation cycles through direct sunlight exposure, while the other two groups were stored in dark conditions (D) and room conditions (Ref) respectively. The nomenclature used for the different curing conditions are shown in Table 1.

Samples submitted to the photo-oxidation cycles (L) were immersed in an aqueous solution of methyl orange (2×10^{-5} M) for 2 h, in dark conditions. The specimens were then allowed to photocatalyze MO for 46 h, for an average period of 8 h per day of direct sun exposure. Similarly, the specimens cured in dark conditions (D) were immersed in the same methyl orange solution for 2 h and then stored in a dark box for 46 h, in which the air was allowed to circulate. Every 48 h the MO solution was replaced by a fresh one. The reference group (Ref) was left to carbonate and harden at room conditions, without being immersed in the methyl orange solution. Finally, an additional fourth group of specimens (Ex) were exposed in open air (Table 1), in a settled area without prior immersion in MO. The specimens were exposed outdoors for two months, where they were exposed daily to direct sun light for an average of 8 h. This experiment included exposure to a high traffic, urban environment with average annual values of air pollutants presented in Table 2. For specimens treated indoors, X-ray diffraction was carried out every week, for a 4-week period, in order to determine the carbonation rate of different mixtures, cured in the three different conditions. The carbonation of specimens exposed in urban environment (Ex) was studied at the end of the 2-month experimental cycle.

Table 2
Mean annual values of air pollutants for the open-air exposure area, as provided by the Hellenic Ministry of the Environment (www.minenv.gr).

Pollutant	NO_2	NO	O_3	SO_2	CO	C	PM_{10}	BTEX
μg/m^3	32	20	57	17	500	22	63	7.5

Powder samples (~1 g) were drilled from a layer of 2 mm thick and subsequently were analyzed. The intensity ratio of the $CaCO_3$ to $Ca(OH)_2$ main diffraction peaks was calculated for each mixture and was plotted versus time and TiO_2 content, in order to obtain an estimate of their relative concentration and the specimens carbonation rate. X-ray powder diffraction (XRD) was carried out in a Siemens D-500 Diffractometer using Cu-K_α radiation (λ = 1.5406 Å, 40 kV, 30 mA). The diffraction spectra were collected in the range of 2–60° 2θ scale, with a step size of 0.03 °/s.

The amount of calcite and portlandite in different mixtures was further evaluated by thermo-gravimetric analysis (DTA/TG), at the end of each experimental cycle [19]. Analyses were carried out in a Perkin-Elmer/Diamond D-6681 thermal analyzer, using a heating rate of 10 °C/min, in air atmosphere.

Furthermore, Micro-Raman spectra were measured in back-scattering configuration using a Renishaw inVia Reflex microscope with an Ar^+ ion laser (λ = 514.5 nm) and a high power near infrared (NIR) diode laser (λ = 785 nm) as excitation sources. The back-scattered Raman signal is detected on a high sensitivity, UV coated, deep depletion CCD detector, while the lowest magnification objective 5× on a Leica DMLM microscope was mostly used to focus the laser light to a sizeable spot of about 8 and 5 μm in diameter at power densities of 0.5 and 0.03 mW/μm^2 for the 785 nm and 514.5 laser lines, respectively. The frequency shifts were calibrated against an internal Si reference. The fluorescence background was subtracted by polynomial fitting and/or cubic spline interpolation routines, while spectral deconvolution was carried out by non-linear least square fitting of the Raman peaks to a mixture of Lorentzian and Gaussian lineshapes.

3. Results and discussion

3.1. Surface properties and microstructure

The examination by SEM of cross-sectioned surfaces of binary pastes cured for 4 weeks, before any experimental cycle, showed that the addition of TiO_2 did not cause any considerable differences in the microstructure of different mixtures. Examination in backscattered electrons (BSE) verified that TiO_2 is evenly distributed within the lime mass, without creating any kind of

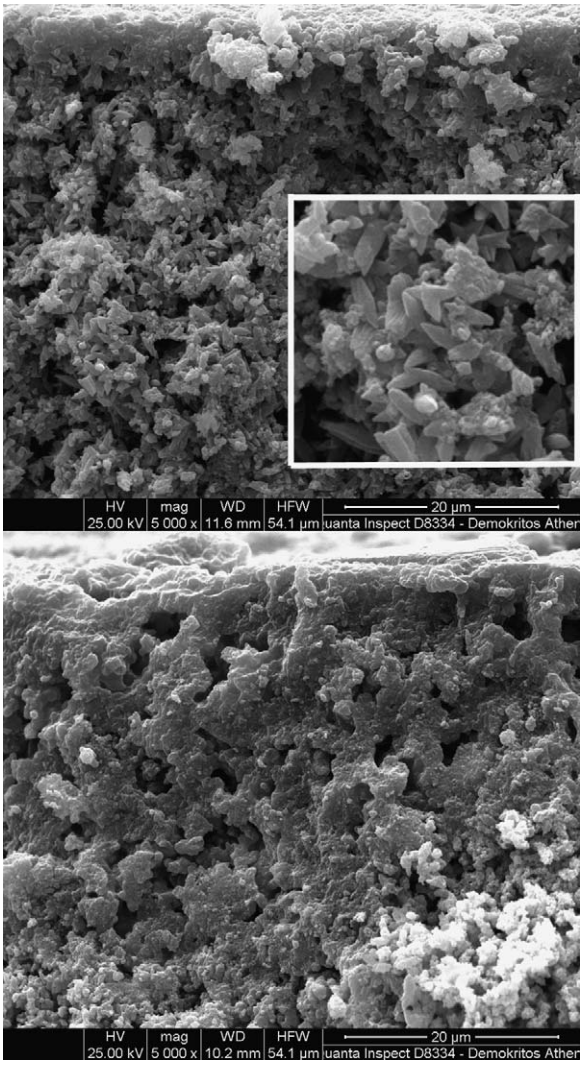

Fig. 1. Scalenohedral calcite crystals of 2–3 μm (seen as inset in the upper image) create a coarse microstructure on the carbonated surface layer of all specimens after the initial 4-week curing (upper image). The initial external layer of 5 μm (formed in Ref and D specimens) extends up to 50–60 μm in specimens L and Ex, after 4-week photocatalysis cycles (lower image).

layering or localized concentrations. Portlandite crystals ($Ca(OH)_2$) dominated the matrix of the pastes, occasionally interrupted by the presence of some irregular polyhedral calcite ($CaCO_3$) crystals formed by precipitation. The amount and the size of calcite crystals was found to increase towards the surface, where scalenohedral calcite crystals in the range of 2–3 μm were formed and created a coarse microstructure (Fig. 1), due to the low degree of carbonation. Finally, on the external surface a uniform and compact carbonated layer of ca. 5 μm was formed. It becomes apparent, therefore, that the total amount of calcite already formed in the surface of the specimens before the execution of any experimental cycles was extremely low.

The evaluation of pore space properties by mercury intrusion porosimetry provided evidence that the addition of titanium dioxide slightly modifies the initial microstructure of pure lime binder (Fig. 2, - see graphs for bulk), however, without affecting their total porosity values. Porosity values of all mixtures after 4 weeks curing and before any experimental cycles, range between 68 and 70% (Table 3). These values are in accordance with data provided elsewhere [35] and describe the pore structure of the pastes that is created during the evaporation of the water initially added in the mixtures (50%, w/w) as well as, the volume changes caused by the dissolution, re-crystallization and carbonation of portlandite [36].

Concerning the bulk of the specimens, which is practically carbonate-free in all specimens, the pore-size distribution graphs show that the addition of titanium dioxide did not affect the mode pore radius values in the area of 200 nm, while it results in the formation of a smooth shoulder at lower pore radii (Fig. 2). More specifically, this shoulder is evident at about 100 nm for mixtures containing 6% (w/w) TiO_2, while two small peaks in pore radius 30 nm and 100 nm are formed in the case of 10%. The above modifications in differential pore size distribution indicate that at low concentrations (up to 3%) TiO_2 particles are packed within the large portlandite grains (0.5–1 μm) and therefore do not have any particular effect on pore size distribution. The addition of 6% (w/w) titanium dioxide (Ca94T6_L) seems totally to fill the pores in the range of 100–300 nm, while above this amount TiO_2 overcomes portlandite particles and creates new, smaller pores in the range of 20–100 nm. The above pore space modifications are attributed to the distribution and packing of TiO_2 particles between portlandite crystals and therefore, results in an increase of pores with smaller pore radius (Fig. 2).

The specimens were further examined by SEM, after the completion of the 28-day and 2 month experimental cycles, respectively. In the case of pastes immersed in MO and cured in dark conditions (D), as well as of those cured in room conditions (Ref), no particular differences were observed in their microstructure. In contrast, the pastes immersed in MO and then photocatalysed under sun light (L), as well as those exposed outdoors exhibited a more extended development of scalenohedral calcite crystals which now exist up to a depth of 1–2 mm from their surface. At the same time the initial external compact layer of 5 μm (in Ref and D specimens) now extends up to 50–60 μm in specimens L and Ex (Fig. 1).

Aiming to investigate the effect of carbonation on the microstructure of the above mixtures, an external 2 mm layer from each sample was removed by microtome, measured by mercury porosimeter and compared to those of the bulk mass. Although the microstructure of this layer is characterized by the presence of coarse pores, the total porosity values decrease in relation to the bulk (Table 3) due to the evolution of the carbonation process. As was also observed in Fig. 2, the external/carbonated layer of the lime-TiO_2 mixtures presents a slight shift of the pore size distribution peak from 200–250 nm to

Table 3
Pore space and mechanical properties of lime-titania pastes.

Sample	Porosity (%)		Water absorption coefficient ($g/m^2 s^{0.5}$) (after 28 days curing (Ref))	F_f (MPa) (after 28 days curing (Ref))
	Non carbonated (bulk (Ref))	Carbonated (2 mm surface layer (L))		
Ca100	68.07	67.13	385.6	2.9
Ca97T3	70.53	68.99	454.8	2.8
Ca94T6	70.28	65.52	477.2	2.8
Ca90T10	69.05	63.10	475.7	2.3

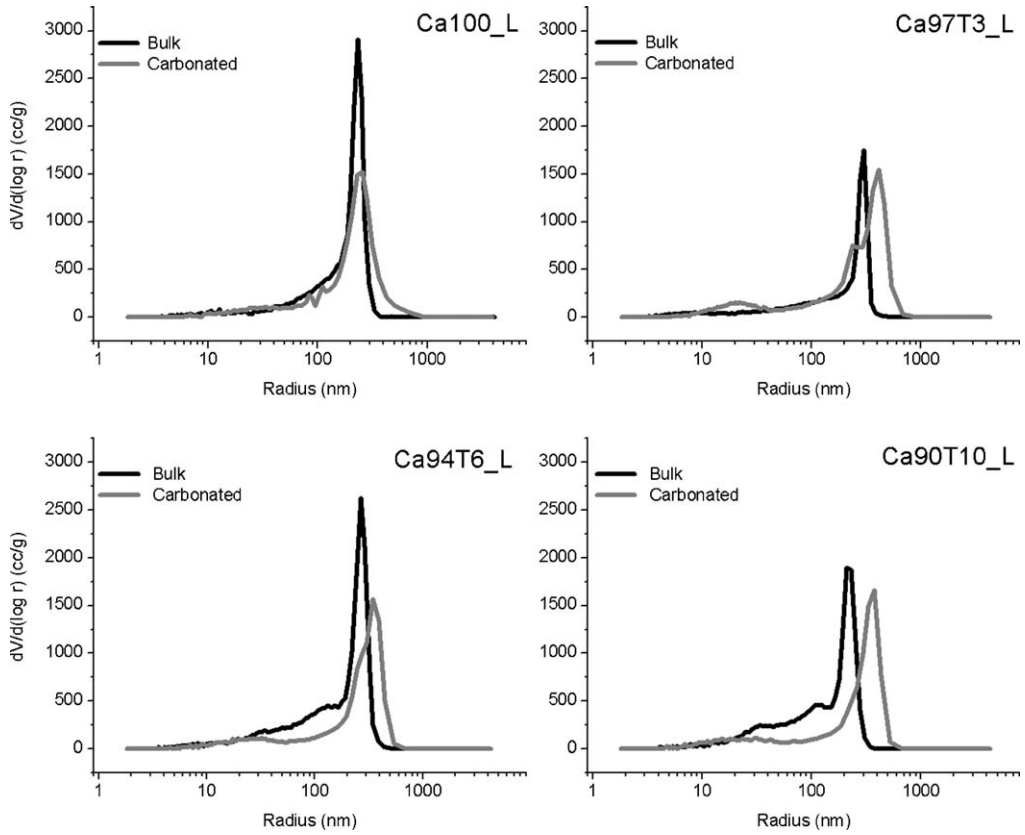

Fig. 2. Differential pore size distribution of carbonated and non-carbonated (indicated as bulk) layers for lime-TiO_2 mixtures, after 4 weeks photocatalysis cycles with methyl orange and direct sunlight exposure. Structure of bulk for each mixture remains constant during hardening (initial 4 weeks) and experimental cycles since it is practically isolated from environment and therefore very little affected by carbonation.

300–400 nm pore radius, while the shoulder at 100 nm disappears in the carbonated mass. In contrast, the pore size distribution of the reference mixture is not particularly affected. The modification of pore space is more intense when the amount of titanium dioxide, which participates in the mixture is increased. The evolution of carbonation in lime mixtures is enhanced by the dissolution of portlandite in the pore solution during immersion (wetting) in the MO solution, the reaction of Ca^{2+} with the dissolved CO_2 and the precipitation of the colloid-size calcium carbonate once a certain super-saturation threshold is reached. The above process gives preference in formation of pores with pore radius below 0.1 μm [37] and results in an additional mass increase, caused by the transformation of portlandite to calcite [17]. Therefore, the evolution of carbonation in lime-TiO_2 specimens affects both their total porosity and pore size distribution (Fig. 2). More specifically, the carbonation of Ca97T3_L specimen results in the formation of a small peak in the range of 10–30 nm and a double peak at 200 and 400 nm pore radius. The same pattern (with a weaker effect) is followed in Ca94T6_L specimens, while Ca90T10_L specimens exhibit a faint and smooth peak at 30 nm along with a single strong peak at 400 nm. The formation of those new peaks at small pore radius (10–30 nm) explains partially the fact that, whereas the carbonation of the lime-TiO_2 pastes results to the formation of coarser pores, the total porosity of the specimens decreases.

The above modification of pore space affects also the absorption and diffusion of carbon dioxide within the body of the binary pastes. According to the model developed by Houst and Wittman [38] for the diffusion of CO_2, the above modifications act beneficially for lime pastes since the resultant microstructure is characterised by an increase of pore volume above 400 nm, which is a critical point for CO_2 uptake and normal diffusion within the lime mass. Finally, the increase of pore volume below 45 nm in lime-TiO_2 mixtures is an indication of the enhanced carbonation of those mixtures (Fig. 2).

During the initial curing, before the cycles, the above mechanism is influenced by the hygric properties of the mixtures, described by water absorption coefficient and water (moisture) retention capacity. As can be seen in Fig. 4, the addition of titanium dioxide results in an increase of water absorption coefficient values between 18 and 24%. The same graph suggests that the effect of TiO_2 on water absorption coefficient values follows a first order exponential trend, and practically reaches its maximum value at 6% (w/w) titanium dioxide. The above phenomenon should be related to both the hydrophilic properties of TiO_2 and the modification of pore space properties in lime mixtures, which result from the addition of TiO_2. This is also evident when moisture content is plotted against TiO_2 content at RH of 95% (Fig. 3), where the curve follows a similar trend to the one of the water absorption coefficient. In the same plot it can be seen that, at lower levels of RH (65%), the different mixtures do not present any significant variability. Thus, it may be concluded that due to hydrophilicity, the amount of titanium dioxide added in lime affects the water amount absorbed in both liquid and vapor states only at high RH % levels, while it exhibits maximum effect at 6% (w/w).

3.2. Internal cohesion–mechanical properties

The slight modification of pore space properties due to the addition of TiO_2 also had a very small effect on the internal cohesion of lime mixtures, regarding the flexural strength values. The addition of TiO_2 up to 6% (w/w) in lime resulted in a decrease of 3% in flexural strength, in relation to pure lime material (2.9 MPa).

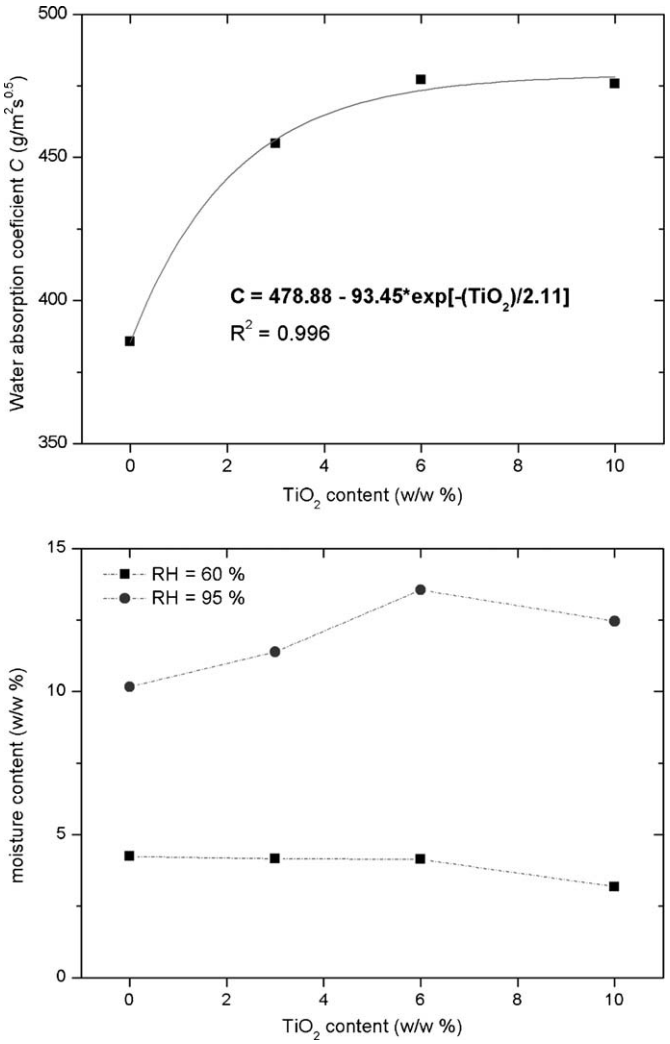

Fig. 3. Exponential fit of water absorption coefficient values, as a function of the amount of TiO_2 added in lime (upper graph), along with moisture retention of lime-TiO_2 mixtures at different relative humidity levels (lower graph).

A more significant decrease (−20%) was observed in mixtures that contain 10% of titanium dioxide. Considering that all lime-TiO_2 mixtures presented a similar microstructure, the strong effect of TiO_2 in the 10% mixture (Ca90Ti10_Ref) should be related to the weakening of the binder matrix due to the significant presence of an inert material (titanium dioxide) within their mass.

3.3. Photocatalytic activity

Photocatalytic experiments reveal a rapid increase of the MO degradation rate under UVA irradiation with increasing TiO_2 content in the modified lime-TiO_2 mixtures (Fig. 4). The MO photodegradation curves for the lime-TiO_2 mortars follow pseudo-first order reaction kinetics, as can be verified by the linear plots of $\ln(C/C_0)$ vs. t shown in Fig. 4, where C_0 is the initial MO concentration.

This suggests that the kinetics could be effectively described by the Langmuir-Hinshelwood model (L-H), frequently applied in modeling the photodegradation of azo dyes [34,39], where the reaction rate R is proportional to the surface coverage S_c (Eq. (1)):

$$R = -\frac{dC}{dt} = k_r \cdot S_c = k_r \cdot \frac{K \cdot C}{1 + K \cdot C}, \quad (1)$$

where k_r is the reaction rate constant, K is the adsorption coefficient of the reactant at the photocatalyst surface and C its

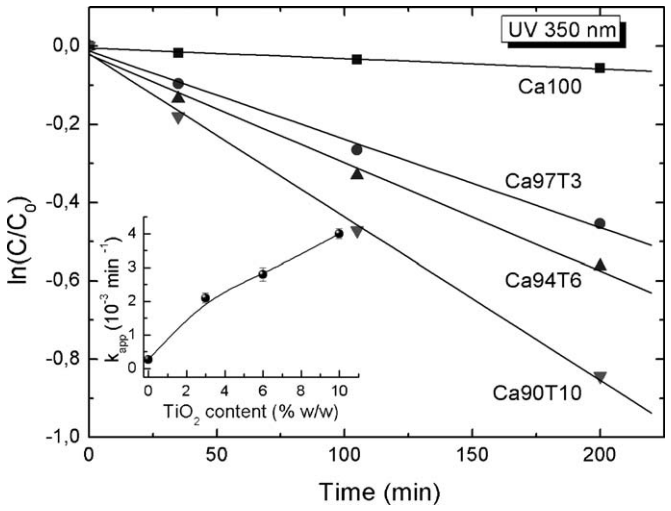

Fig. 4. Photodegradation kinetics of methyl orange under UVA (350 nm) irradiation for the TiO_2 modified lime mortar samples compared to the unmodified one. The inset displays the variation of the apparent first order reaction constants (k_{app}) as a function of the TiO_2 content. The line is a guide to the eye.

concentration. Integration of Eq. (1) at low concentrations of the organic pollutant ($KC << 1$) leads to an apparent first order equation (Eq. (2)):

$$\ln\left(\frac{C}{C_0}\right) = -k_r \cdot K \cdot t = -k_{app} \cdot t, \quad (2)$$

with k_{app} being the apparent first-order reaction constant. The values of k_{app} for the different mixtures, derived from linear fitting of the $\ln(C/C_0)$ vs. t data, to Eq. (2), are shown in the inset of Fig. 4. Changes in k_{app} are attributed, via Eq. (2), to the corresponding variations in the K values, i.e. to the different absorption of the reactant on the photocatalyst surface or equivalently to the different surface coverage S_c. A systematic increase in the MO photodegradation rate is thus evidenced upon increasing the TiO_2 content in the lime pastes, reflecting the increased concentration of the active photocatalytic nanoparticles.

In order to check the potential reusability composite photocatalyst, we have performed a series of five photocatalytic cycles using the material that exhibits the highest activity. The MO photodegradation as well as the first-order reaction constants k_{app} do not vary significantly and the results were reproducible within 5%, despite the carbonation process.

3.4. Carbonation process

The evaluation of the diffraction patterns derived from specimens cured and treated in the laboratory (series Ref, D, L) showed (Fig. 5) that there existed an advancement of carbonation in the L specimens compared to the rest. This became evident from the evaluation of the intensity ratio of calcite to portlandite (Cc/Ptl) main peaks. The same pattern is observed in the intensity ratio plot for mixtures exposed outdoors (Fig. 5). In both plots, the intensity ratio values of all lime-TiO_2 mixtures fluctuate around 7.5 and do not seem to be affected by the amount of titanium dioxide that participates in the mixture.

In contrast, the immersion of the binary mixtures in the aquatic solution of MO without photocatalysis did not cause any effect on the diffusion of atmospheric carbon dioxide into the mortar mass. The above mixtures exhibited the lowest carbonation rate. The latter was expected, since the diffusion coefficient of carbon dioxide in aqueous solutions is much lower than in air [14,17].

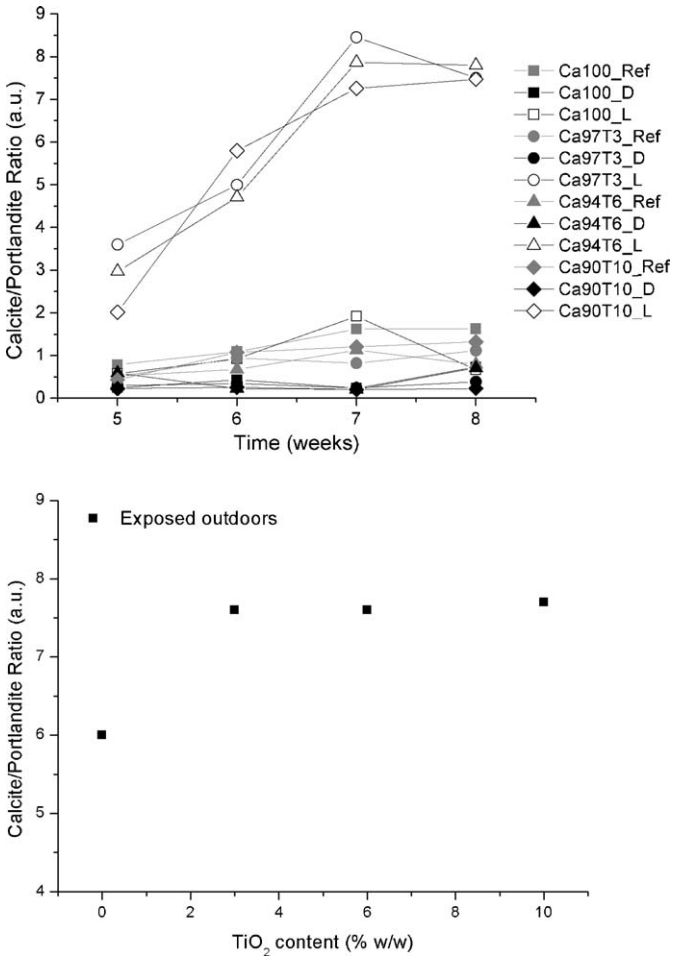

Fig. 5. Calcite ($CaCO_3$) to portlandite ($Ca(OH)_2$) main-peak intensity ratios for different mortar mixtures photocatalyzed in laboratory for four weeks (upper graph), and calcite/portlandite main-peak intensity ratios for mixtures exposed outdoors for 2 months, derived from X-ray diffraction patterns (lower graph).

The above findings confirmed the initial assumption that CO_2 release during photocatalysis could have a positive effect on the carbonation process of lime-TiO_2 mixtures.

The quantitative determination of the carbonate phases formed in each mixture through thermal analysis (TG%) reinforced the diffraction results and revealed that photocatalysis, both in laboratory and outdoors conditions resulted in an increase in the amount of calcium carbonate formed in an external layer of at least 2 mm in all lime-TiO_2 mixtures (Fig. 6).

The photo-oxidation of methyl orange for 4 weeks resulted in an acceleration in the carbonation process, through the release of additional amounts of CO_2. This procedure produced the same amount of $CaCO_3$ as the specimens exposed outdoors for 2 months.

Although the procedure followed in the laboratory does not correspond to the actual mechanism of the natural carbonation process that takes place outdoors, the results show that the amount of carbonate phases increase proportionately to the amount of TiO_2 and therefore, the photo-oxidation ability of the lime-TiO_2 mixtures. The same trend is also evident in mixtures exposed outdoors, with the exception of the mixture Ca97T3_Ex, which contained the lowest amount of TiO_2.

It is therefore apparent that CO_2, the final product of the photocatalytic process is responsible for the acceleration observed in the carbonation process, while the super-hydrophilic properties of TiO_2 do not obstruct the above mechanism. In contrast, the increased water vapor adsorption ability of lime-TiO_2 pastes could also contribute to the reaction between calcium hydroxide particles and carbon dioxide at room temperature (20–25 °C) [40].

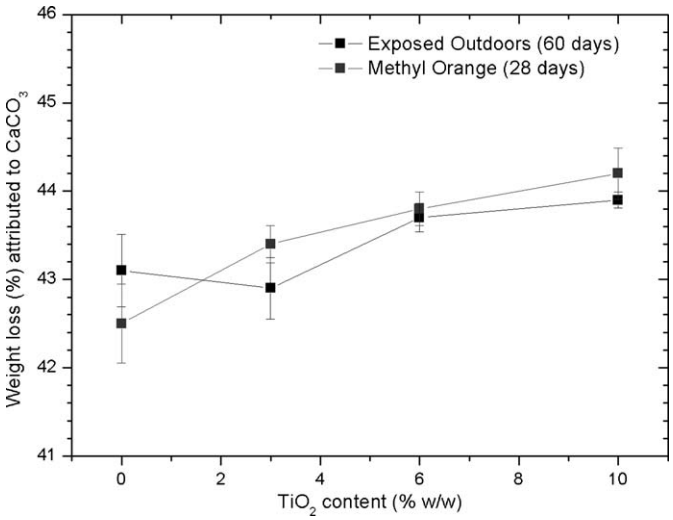

Fig. 6. Carbonates ($CaCO_3$) amount formed in an external layer of 2 mm in specimens exposed outdoors for 2 months and, for those immersed in methyl orange and photocatalysed by direct exposure to sun-light for 28 days ($n = 3$).

3.5. Phase composition/carbonation by micro-Raman

Micro-Raman spectroscopy has been employed subsequently to determine the phase composition and the effect of carbonation in the lime-TiO_2 binary mixtures, subjected to photo-oxidation under direct sunlight. Fig. 7a and b displays the corresponding Raman spectra on polished surfaces of the cross-section of the lime specimens at a depth of 0.5 mm from the exposed surface, using NIR (785 nm) excitation. The formation of calcite as the major calcium carbonate phase can be clearly identified at this depth for all samples through the observation of the distinct low frequency lattice (external) modes of calcite at 154 and 280 cm^{-1}, as well as the characteristic internal vibrations of the CO_3 groups at 712 cm^{-1}(ν_4-symmetric CO_3 deformation) and 1086 cm^{-1} (ν_1-symmetric CO_3 stretching) [41]. In addition, the presence of a weak mode at 205 cm^{-1}, most clearly resolved for the Ca94T6 sample, as well as the asymmetric lineshape of the 712 cm^{-1} band indicate the presence of the aragonite polymorphic phase in the lime-TiO_2 pastes [42]. Spectral fitting of the latter composite band reveals two weak peaks at approximately 701 and 705 cm^{-1} stemming from the aragonite phase [43], and a sharper and more intense one at 712 cm^{-1} due to calcite (Fig. 7a). Based on previous Raman calibration results of the intensity ratio (I_{712}/I_{701}) in calcite/aragonite binary mixtures [44] and the ratio values determined from the area of the corresponding bands, a rough estimate of the weight fraction of the two calcium carbonate phases can be obtained. The resulting amounts of aragonite range from about 20% for Ca94T6 to 10–15% for the Ca100 and Ca90T10 specimens. It should be noted that the identification of aragonite was not possible by XRD within the 2 mm upper layer of the lime mortars, indicating that on average the amount of aragonite within this volume should be near the XRD detection limit (3–5%). This variation complies with previous micro-Raman results showing a diverse depth distribution of aragonite in lime mortars [42]. The formation of aragonite can be related to the dissolution and recrystallisation of carbonates during experimental cycles with MO treatment [45]. However, this should be regarded as a precursor phase of calcium carbonate, which is gradually transformed to calcite.

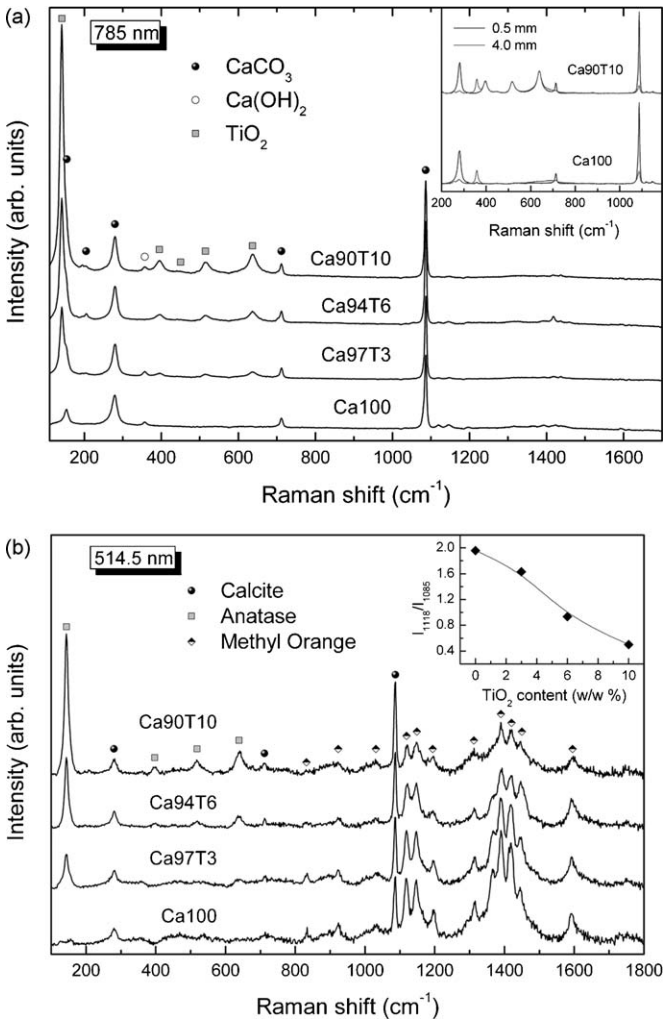

Fig. 7. (a) Micro-Raman spectra of the photo-oxidized lime pastes at a depth of 0.5 mm from the exposed surface, at 785 nm. The inset compares the Raman spectra of Ca100 and Ca90T10, at depths of 0.5 and 4 mm. (b) Micro-Raman spectra of the photo-oxidized lime pastes at a depth of 0.5 mm and 514.5 nm laser excitation, after subtraction of the fluorescence background. The inset displays the variation of the intensity ratio I_{1118}/I_{1086} as a function of the TiO_2 content.

Furthermore, the Raman spectra of the lime-TiO_2 mixtures exhibit the characteristic vibrational modes of the nanocrystalline anatase TiO_2 phase: the most intense E_g modes centered at 144 and 639 cm^{-1}, the B_{1g} mode at 397 and the composite band stemming from the overlap of the A_{1g} with the B_{1g} mode at 519 cm^{-1} [46]. A very weak mode at 445 cm^{-1} due to the minor rutile phase comprised in the initial Degussa-P25 powder can be also traced for the mixtures with the higher TiO_2 loading. The Raman intensity of the titania bands scales linearly with the TiO_2 content in the binary mixtures, supporting the efficient introduction of nanocrystalline titania in the lime mass.

The presence of portlandite also can be testified at this depth of the lime specimens, through the observation of a relatively weak band at 357 cm^{-1}, corresponding to the most intense A_{1g} lattice vibration (translational –OH displacement) of $Ca(OH)_2$ [47]. The intensity of this band varies appreciably both between the different samples and for different areas of the same sample (under the laser spot size of approximately 8 μm attained with the lowest magnification objective of ×5 at the 785 nm Raman spectra), implying an inhomogeneous distribution of portlandite crystals at this spatial scale for the upper lime layers. On the other hand, a pronounced increase of the portlandite 357 cm^{-1} Raman intensity is observed at a depth of 4 mm from the sample surface that allows resolving also the weaker E_g lattice mode at 254 cm^{-1} (–OH rocking motion) of $Ca(OH)_2$, as shown in the inset of Fig. 7a. This variation is accompanied by a drastic reduction of the intensity of the calcite Raman peaks, confirming the termination of the carbonation process at this depth.

Fig. 7b compares the micro-Raman spectra of the lime specimens at a depth of 0.5 mm using the 514.5 nm laser excitation. In that case, an intense fluorescence background, stemming from the emission of both the MO reactant [48] and the mineral matrix [49], has been found to hamper the resolution of the Raman peaks compared to the corresponding NIR Raman spectra. Subtraction of the fluorescent background from the Raman spectra reveals that apart from the intense calcite and anatase Raman bands, a series of Raman peaks is resolved at higher wavenumbers (>1100 cm^{-1}), hardly discernible in the NIR Raman spectra (Fig. 7b). These peaks can be identified with the MO Raman vibrations in aqueous solutions, resonantly enhanced in the visible region by the 514.5 nm excitation that approaches the absorption maximum of MO at 466 nm [48]. Comparison of the Raman spectra between the different lime specimens shows a substantial decrease of the intensity of the MO vibrations with respect to both the calcite and anatase Raman bands. Spectral fitting of the Raman peaks has been accordingly applied to determine the intensity ratio of the calcite 1086 cm^{-1} (symmetric CO_3 stretching) band to the MO 1118 cm^{-1} (SO_3^- stretching) vibration from the corresponding peak areas for the different specimens, as shown in the inset of Fig. 7b. An almost linear drop in the intensity ratio I_{1118}/I_{1086} is thus derived as a function of the TiO_2 content. This variation can be explained by the decrease of the MO concentration due to the enhanced TiO_2 photocatalytic action for the binary mixtures with the higher titania loading and the simultaneous release of higher amounts of CO_2 that contribute to calcite formation, providing further evidence for the promotion of lime carbonation by the TiO_2 photocatalytic process.

4. Conclusions

The analysis of the results indicates that titanium dioxide can be combined with lime and create a compatible binding material and therefore, can be used to produce new mortar mixtures for conservation purposes.

Lime-TiO_2 binary mixtures exhibited a considerable acceleration in the carbonation rate, due to the increase of carbon dioxide concentration, resultant from the photocatalysis (photo-oxidation) of the organic pollutants both in the laboratory (methyl orange) and outdoor environments. The addition of TiO_2 to lime mortars ensures that when photocatalysis is accomplished, a higher concentration of CO_2 in gas form is achieved on the surface of the material.

The photocatalytic activity of the modified materials increases according to the increased percentage of TiO_2 in the lime-TiO_2 mortar mixtures, presenting the best performance between 6 and 10% (w/w). The concentration around 6% (w/w) seems to be the optimum amount for the replacement of lime binder, since it combines a high photocatalytic rate with minimal alteration of physical and mechanical properties of the titania modified lime mortars.

Although the photocatalysis is a surface phenomenon, the CO_2 produced is dissolved in water vapors and absorbed in the mortar mass through capillarity to depths reaching more than 2 mm. Furthermore, the addition of TiO_2 in the entire mass ensures the potential of decomposition of organic pollutants even after the degradation of the initial surface of the mortars.

Therefore, it is clear that the addition of TiO_2 in lime-based repair mortars is beneficial, since it can ensure increased durability

against organic pollutants, improved aesthetic characteristics, increased depth of carbonation and accelerated carbonation rate.

Acknowledgements

This work has been partially funded by the project PENED 03EΔ 963, 2003. The project is co-financed by 75% of public expenditure through the EC - European social fund, 25% of public expenditure through Ministry of Development–General Secretariat of Research and Technology and through the private sector, under measure 8.3 of operational programme "Competitiveness" in the 3rd Community Support Programme. The authors would like to thank Dr G. Romanos, researcher at the Institute of Physical Chemistry for his contribution in mercury intrusion porosimetry.

References

[1] C. Saiz-Jimenez, Atm. Environ. 27B (1993) 77–85.
[2] C. Saiz-Jimenez, P. Brimblecombe, D. Camuffo, R.A. Lefèvre, R. Van Grieken, in: C. Saiz-Jimenez (Ed.), Air Pollution and Cultural Heritage, Balkema Publishing, Leiden, 2004, pp. 91–109.
[3] C. Sabbioni, in: P. Brimblecombe (Ed.), The Effects of Air Pollution on the Built Environment: Air Pollution Reviews, vol. 2, Imperial College Press, London, 2003, pp. 63–106.
[4] J. Watt, R. Hamilton, in: P. Brimblecombe (Ed.), The Effects of Air Pollution on the Built Environment: Air Pollution Reviews, vol. 2, Imperial College Press, London, 2003, pp. 63–106.
[5] J. Simao, E. Ruiz-Agudo, C. Rodriguez-Navarro, Atm. Environ. 40 (2006) 6905–6917.
[6] J. Reyes, B. Hermosin, C. Saiz-Jimenez, Org. Geochem. 37 (2006) 2019–2025.
[7] A. Bonazza, C. Sabbioni, N. Ghedini, Atm. Environ. 39 (2005) 2607–2618.
[8] R.W. Lanting, in: S.D. Lee, T. Schneider, L.D. Grant, P.J. Verkerk (Eds.), Aerosols, Lewis Publishers, Michigan, 1986, pp. 923–932.
[9] Y. Bai, G.E. Thompson, S. Martinez-Ramirez, Building Environ. 41 (2006) 486–491.
[10] B.O. Fobe, G.J. Vleugels, E.J. Roekens, R.E. van Grieken, B. Hermosin, J.J. Ortega-Calvo, A. Sanchez del Junco, C. Saiz-Jimenez, Environ. Sci. Technol. 29 (1995) 1691–1701.
[11] A. Rabl, Environ. Impact Assess. Rev. 19 (1999) 361–385.
[12] Al. Bonazza, P. Brimblecombe, C.M. Grossi, C. Sabbioni, Environ. Sci. Technol. 41 (2007) 4199–4204.
[13] M.V. Diamanti, M. Ormellese, M.P. Pedeferri, Cem. Concr. Res. 38 (2008) 1349–1353.
[14] G. Sabbioni, G. Zappia, N. Ghedini, G. Gobbi, O. Favoni, Atmos. Environ. 32 (1997) 215–223.
[15] K. van Balen, E.E. Toumbakari, M.T. Blanco-Varela, J. Aquilera, F. Puertas, A. Palomo, C. Sabbioni, C. Riontino, G. Zappia, Research Report for project ENV4-CT95-0096, Diractorate-General XII for Science, Research and Development, 1999.
[16] G. Sabbioni, G. Zappia, C. Riontino, M.T. Blanco-Varela, J. Aguilera, F. Puertas, K. van Balen, E.E. Toumbakari, Atmos. Environ. 35 (2001) 539–548.
[17] D.R. Moorehead, Cem. Concr. Res. 16 (1986) 700–708.
[18] O. Cazalla, C. Rodriguez-Navarro, E. Sebastian, G. Cultrone, M.J. De la Torre, J. Am. Ceram. Soc. 83 (2000) 1070–1076.
[19] R.M.H. Lawrence, T.J. Mays, P. Walker, D. D'Ayala, Thermochim. Acta 444 (2006) 179–189.
[20] E. Hansen, E. Doehne, J. Fidler, J. Larson, B. Martin, M. Matteini, C. Rodriguez-Navarro, E.S. Pardo, C. Price, A. de Tagle, J.M. Teutonico, N. Weiss, Rev. Conserv. 4 (2003) 13–25.
[21] P. Baglioni, L. Dei, F. Piqué, G. Sarti, E. Ferroni, Stud. Conserv. 42 (1997) 43–54.
[22] F. Medici, G. Rinaldi, Environ. Eng. Sci. 19 (2002) 271–276.
[23] O. Cizer, K. Van Balen, J. Elsen, D. Van Gemert, 2nd International Conference on Accelerated Carbonation for Environmental and Materials Engineering (ACEME08), Rome, (2008), pp. 149–158.
[24] A. Fujishima, X. Zhang, D.A. Tryk, Surf. Sci. Rep. 63 (2008) 515–582.
[25] M. Lackhoff, X. Prieto, N. Nestle, F. Dehn, R. Niessner, Appl. Catal. B 43 (2003) 205–216.
[26] T. Yuranova, V. Sarria, W. Jardim, J. Rengifo, C. Pulgarin, G. Trabesinger, J. Kiwi, J. Photochem. Photobiol. A 188 (2007) 334–341.
[27] Rachel, M. Subrahmanyam, P. Boule, Appl. Catal. B 37 (2002) 301–308.
[28] EN 1925. Natural stone test methods – determination of water absorption coefficient by capillarity, British Standard Institution, 1999.
[29] C. Fortes-Revilla, S. Martínez-Ramírez, M.T. Blanco-Varela, Cem. Concr. Compos. 28 (2006) 458–467.
[30] C. Baiocchi, M.C. Brussino, E. Pramauro, A.B. Prevot, L. Palmisano, G. Marcì, Int. J. Mass Spectrosc. 214 (2002) 247–256.
[31] K. Dai, H. Chen, T. Peng, D. Ke, H. Yi, Chemosphere 69 (2007) 1361–1367.
[32] P. Falaras, I.M. Arabatzis, T. Stergiopoulos, M.C. Bernard, Int. J. Photoenergy 5 (2003) 123–130.
[33] H. Gerischer, A. Heller, J. Phys. Chem. 95 (1991) 5261–5267.
[34] K. Rajeshwara, M.E. Osugi, W. Chanmanee, C.R. Chenthamarakshan, M.V.B. Zanoni, P. Kajitvichyanukul, R. Krishnan-Ayer, J. Photochem. Photobiol. C 9 (2008) 171–192.
[35] M. Arandigoyen, J.I. Alvarez, Appl. Surf. Sci. 252 (2006) 8077–8085.
[36] R.M. Lawrence, T.J. Mays, S.P. Rigby, P. Walker, D. D' Ayala, Cem. Concr. Res. 37 (2007) 1059–1069.
[37] C. Rodriguez-Navarro, O. Cazalla, E. Elert, E. Sebastian, Proc. R. Soc. A 458 (2002) 2261–2273.
[38] Y.F. Houst, F.H. Wittman, Cem. Concr. Res. 24 (1994) 1165–1176.
[39] I.K. Konstantinou, T.A. Albanis, Appl. Catal. B 49 (2004) 1–14.
[40] D.T. Beruto, R. Botter, J. Eur. Ceram. Soc. 20 (2000) 497–503.
[41] H.N. Rutt, J.H. Nicola, J. Phys. C 7 (1974) 4522–4528.
[42] S. Martinez-Ramirez, S. Sanchez-Cortes, J.V. Garcia Ramos, C. Domingo, C. Fortes, M.T. Blanco-Varela, Cem. Concr. Res. 33 (2003) 2063–2068.
[43] R. Frech, E.C. Wang, J.B. Bates, Spectrochim. Acta A 36 (1980) 915–919.
[44] C.G. Kontoyannis, N.V. Vagenas, Analyst 125 (2000) 251–255.
[45] S. Valadas, D. Tavares, J. Coroado, A.S. Silva, J. Pedro, J. Mirão, A. Candeias, Mater. Sci. Forum 587–588 (2008) 1019–1023.
[46] V. Likodimos, T. Stergiopoulos, P. Falaras, J. Kunze, P. Schmuki, J. Phys. Chem. C 112 (2008) 12687–12696.
[47] S. Ekbundit, K. Leinenweber, J.L. Yarger, J.S. Robinson, M. Verhelst-Voorhees, G.H. Wolf, J. Solid State Chem. 126 (1996) 300–307.
[48] K. Machida, H. Lee, A. Kuwae, J. Raman Spectrosc. 9 (1980) 198–201.
[49] B.J. Bozlee, A.K. Misra, S.K. Sharma, M. Ingram, Spectrochim. Acta A 61 (2005) 2342–2348.